Scripta Materialia 178 (2020) 176–180

Contents lists available at ScienceDirect

Scripta Materialia

journal homepage: www.elsevier.com/locate/scriptamat

Microstructural characterization of the protective oxide scale forming on Ni–25Cr–xMn (x = 0.5, 1 and 1.5% wt) in a 200 Pa O_2 environment at 1050 °C

T. Perez[a], J. Ghanbaja[a], S. Mathieu[a,*], L. Latu-Romain[b], M. Vilasi[b], Y. Wouters[b]

[a] Université de Lorraine, CNRS, IJL, F-54000 Nancy, France
[b] University of Grenoble Alpes, CNRS, SIMaP, F-38000 Grenoble, France

ARTICLE INFO

Article history:
Received 30 April 2019
Revised 8 November 2019
Accepted 13 November 2019

Keywords:
Oxidation
Nickel alloys
Spinel
Microstructure
High-resolution electron microscopy (HREM)

ABSTRACT

To clarify the influence of manganese on the oxidation behavior of Ni–Cr alloys, high resolution transmission electron microscopy was used to examine the microstructure and chemistry of oxide scales forming at 1050 °C on Ni–25Cr–xMn (x = 0.5, 1 and 1.5% wt) in 200 Pa O_2. The scales consisted of two layers of chromia and one layer of spinel $Mn_{1+x}Cr_{2-x}O_4$. The internal layer exhibited an equiaxed grain structure, whereas columnar grains developed in the outer layer. The results demonstrated that the spinel composition at the chromia-spinel interface was similar regardless of the manganese concentration.

Chromia-forming nickel-based alloys are commonly used for components that encounter oxidizing and reducing environments at high temperatures because of their thermodynamic stability and the low rate of chromia growth [1,2]. The minor alloying elements, Al, Mn, Si, Ti, and Y [1,3,4], have large effects on the chromia growth rate by modifying the transport properties of the scale [5,6]. Focusing the present study on the Mn effect, it was shown [4] that Mn addition increases the oxidation kinetics by a factor of 1.5 for a long time in isothermal conditions. It is also known [3,4,7] that a small amount of manganese (lower to 1% wt) in Ni–Cr alloys allows the formation of a spinel layer at the oxide/gas interface with a composition reported to fall in the range from $MnCr_2O_4$ to Mn_3O_4 [8]. Although the presence of this oxide is frequently noticed [3,4,9,10–12], the latter is rarely considered when debating the oxidation mechanism of nickel-based alloys. However, manganese addition increases the overall oxidation rate as well as the chromia growth rate [3,4] and decreases the oxide scale adhesion [3,4,11]. Ledoux et al., using photoelectrochemistry, has also proposed, based on the observation of a systematic change of chromia semiconductivity when the spinel formed, that the manganese chromium spinel might control the boundary conditions at the chromia/spinel interface [9]. These authors showed in this way a change in the ratio of point defect concentrations. In addition, Holcomb's calculation [13] showed that the presence of $MnCr_2O_4$ on top of a chromia scale should contribute to a decrease in the oxidation of chromia in volatile CrO_3 at high temperatures.

Consequently, there is a strong interest to accurately characterize the structure and composition of the oxide scale forming on model Ni–25Cr–xMn (x = 0.5, 1 and 1.5% wt) alloys; notably, to accurately define the local equilibrium at the chromia/spinel interface. This is carried out in the present study using HR-TEM and STEM techniques for alloys oxidized for 1 h in 200 Pa O_2.

Three model alloys were prepared by high-frequency melting under argon gas (details can be found elsewhere [4]) according to three compositions of Ni–25Cr–xMn with x = 0.5, 1 and 1.5 in weight percent. The ingots were then heat-treated for 12 h at 1000 °C under argon for homogenization and avoid segregation. The samples were oxidized in an environmental scanning electron microscope (FEI Quanta 200 FEG ESEM) equipped with a 1400 °C hot stage under an atmosphere of pure O_2 ($O_2 \geq 99.995\%$) at 200 Pa. The hot stage was heated to the experimental temperature of 1050 °C under 200 Pa O_2 at the rate of 50 °C min^{-1}. The furnace was equipped with a specific thermocouple that allowed a precise measure of the sample temperature [14]. When the target temperature was reached, the samples were heated isothermally and observed in situ for 1 h [4]. After exposure, cross sections of the oxide layers were obtained by extracting from the oxidized samples thin lamellas by a dual focused ion beam (FIB) scanning

* Corresponding author.
E-mail addresses: stephane.mathieu@univ-lorraine.fr, stephane.mathieu@ijl.nancy (S. Mathieu).

https://doi.org/10.1016/j.scriptamat.2019.11.030
1359-6462/

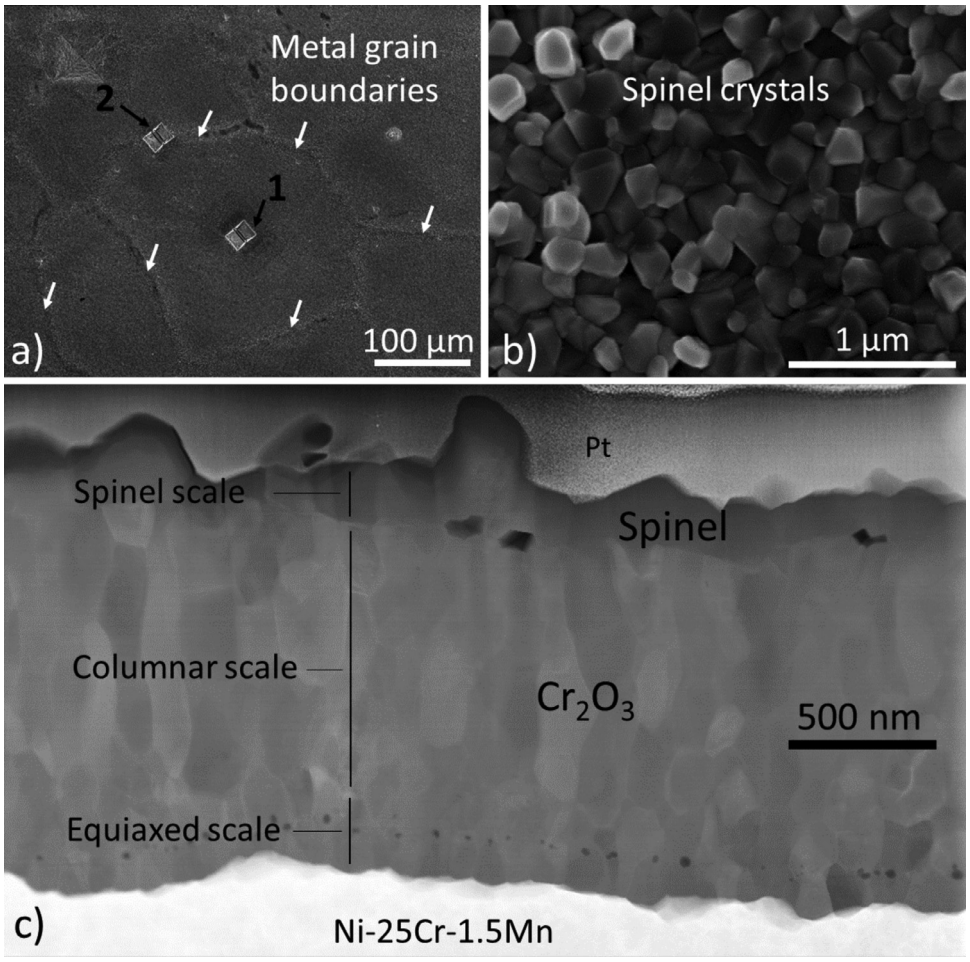

Fig. 1. Observations of the Ni–25Cr–1.5Mn oxidized for 1 h in 200 Pa O_2 after the thin foil extractions (marked 1 and 2): (a) surface at low magnification (SEM-SE); (b) surface at high magnification (SEM-SE); (c) cross section relative to location 1 (STEM dark field mode) showing equiaxed chromia grains at the metal/oxide interface, a thick layer of columnar chromia grains and a top continuous spinel layer.

electron microscope (Helios Nanolab 600i) system using the in situ lift-out technique. Two lamellas of approximately 50 nm thickness were prepared for each sample, one on top of a metal grain boundary and the other on top of a metal grain. A high resolution transmission electron microscope (JEOL ACCEL ARM 200F-Cold FEG) with a (C_s) spherical aberration probe corrector was used to perform the microstructure characterization. The point resolution was in TEM mode 0.12 nm and in STEM mode 0.083 nm. The TEM was operated at an acceleration voltage of 200 kV. The chemical analyses were realized with an energy dispersive X-ray (EDX) spectrometer (JEOL Centurio EDS 1 sr) and an electron energy loss spectrometer EELS (GIF QUANTUM ER) coupled to the electron microscope. Oxygen was quantified by stoichiometry.

Surface observations of the sample Ni–25Cr–1.5Mn after 1 h of oxidation at 1050 °C in 200 Pa of dioxygen are presented in Fig. 1a. The footprint of the initial microstructure (coarse grains of approximately 150–200 µm) remains visible, reflecting the different chromia growth rate on the grain and at the grain boundary (GB). The location where the FIB thin slices were extracted can be seen in Fig. 1a. The surface observations for Ni–25Cr–0.5Mn and Ni–25Cr–1Mn are very similar to the one presented in Fig. 1b for Ni–25Cr–1.5Mn. Crystallites of manganese chromium spinel entirely covered the sample surface regardless of the initial Mn concentration. Cross sections of the Ni–25Cr–1Mn sample were observed in STEM mode. The STEM micrograph (Fig. 1c) clearly shows the multi-layered structure. The scale consists of a thin layer of equiaxed chromia grain at the metal/oxide interface, a thick layer of columnar chromia grain and finally a thin spinel layer on top. Latu-Romain et al. [15] and Lech et al. [16] also noticed that the chromia layers formed on pure chromium and on polycrystalline Ni-based superalloys can be divided into two parts based on their equiaxed and columnar microstructures. Small voids were observed in the equiaxed layer. It can be suggested that their locations correspond to the initial metal-atmosphere interface and represent the separation between the inward and the outward growth [17] of this equiaxed layer. The peculiar morphology of the latter can result of the oxide nucleation mechanism as proposed by Zhou [18]. The spinel layer was only one grain thick in all observations made. Fewer and larger voids are also locally present at the chromia/spinel interface of all Ni–25Cr–xMn alloys.

Fig. 2 displays the scale of the Ni–25Cr–1Mn both on top of a metal grain and on top of a metal grain boundary in bright field mode. A triplex oxide scale composed of the continuous spinel layer at the oxide/gas interface with a thicker duplex columnar/equiaxed chromia layer underneath was observed in both cases. On top of the metal grain, the thickness of the oxide scale is approximately 980 nm whereas it reaches 1620 nm on top of the metal GB. The thickness measurements of each subscale were made on the six FIB lamellas (Fig. 2c). Each data point corresponds to the average of 10 measurements. The triplex oxide scale formed on GB is systematically thicker than the scale that develops on top of grains. However, the oxidation rate on top of the metal grain is

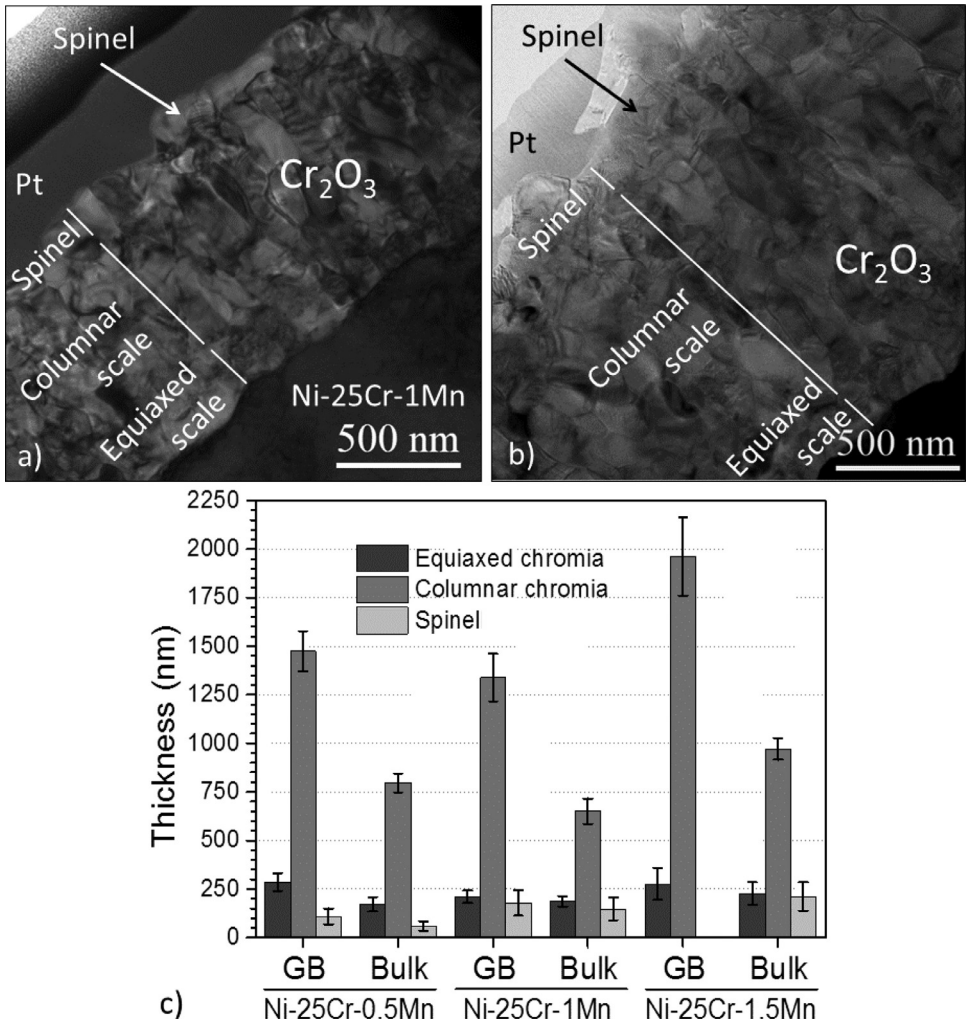

Fig. 2. Cross section TEM bright field micrographs of the oxide scale on Ni–25Cr–1Mn formed after 1 h at 1050 °C in 200 Pa O_2: (a) on top of a metal grain; (b) on top of a metal grain boundary (GB). (c) Thickness measurement results of the three identified layers according to the Mn addition to Ni–25Cr and to the location of the extracted FIB lamellas.

more or less the same whatever the Mn concentration in the bulk. The thickness of the equiaxed chromia layer slightly increases with manganese addition whereas the effect of manganese on the thickness of the columnar chromia layer is less clear. It should be added that due to the level of stresses of chromia grown on Mn free Ni–25Cr it was not possible to extract FIB lamella in the Ni–25Cr alloy that was taken as the reference because all of the lamella broke during extraction. Nevertheless, as reported by Simon et al., the microstructure in these conditions should be only equiaxed at 200 Pa of oxygen [19,20]. Overall, an increase in Mn results in a slight increase of the size of spinel crystallites. This influence is peculiarly highlighted at the GB location. Due to experimental difficulties with the FIB, It was not possible to measure the size of the spinel crystallites at GB for Ni–25Cr–1.5Mn. Nevertheless, the latter was determined from surface observation in [4], which demonstrated the crystallites' size increased with Mn content.

Energy dispersion spectrometry (EDS) and electron energy loss spectrometry (EELS) were carried out to obtain quantitative and qualitative information on the spinel chemistry. The changes of the chromium and manganese atomic percentages in the cation sub-lattice across the spinel/chromia interface are reported for Ni–25Cr–1Mn in Fig. 3. On top of the metal grain (Fig. 3c), the manganese signal continuously decreased through the spinel grain up to approximately 33 ± 2% at the chromia-spinel interface, similar to what was obtained for Ni–25Cr–0.5Mn and Ni–25Cr–1.5Mn on top of metal grains. This shows the composition of $MnCr_2O_4$ is in equilibrium with the chromia scale as expected from the thermodynamic assessment of Jung [21]. At GB (Fig. 3d) and because of the STEM technique that required the surface to be perpendicular to the electron beam, the chromia and spinel crystals overlap and the compositions profile is less accurate, hindering any conclusion about the existence of a thermodynamic equilibrium at these locations. The very low amount of manganese in the chromia scale did not' permit its quantification. Thus, for the spinel formed on top of the grains, the maximum atomic ratio Mn/Cr is 0.724 *vs* 0.5 for a composition that corresponds to $MnCr_2O_4$. This ratio increases to 2.125 for spinel located on top of the metal GB, revealing the higher manganese flow at this location. The EELS results (not illustrated here) qualitatively showed the contribution of Mn^{III} was higher in the spinel grains located on top of the metal GB; i.e., that manganese substitutes more for chromium on the octahedral site of the $MnCr_2O_4$ structure at GB.

Selected area electron diffraction (SAED) (Fig. 4b) allowed for the determination of the spinel crystalline structure. Spinel crystallized in the cubic spinel structure (Fd-3 m with $a = 0.846$ nm). The literature [22] indicates that for manganese chromium spinel at room temperature, the expected crystal structure would be tetragonal (I41/amd) or cubic (Fd-3m) according to the cations

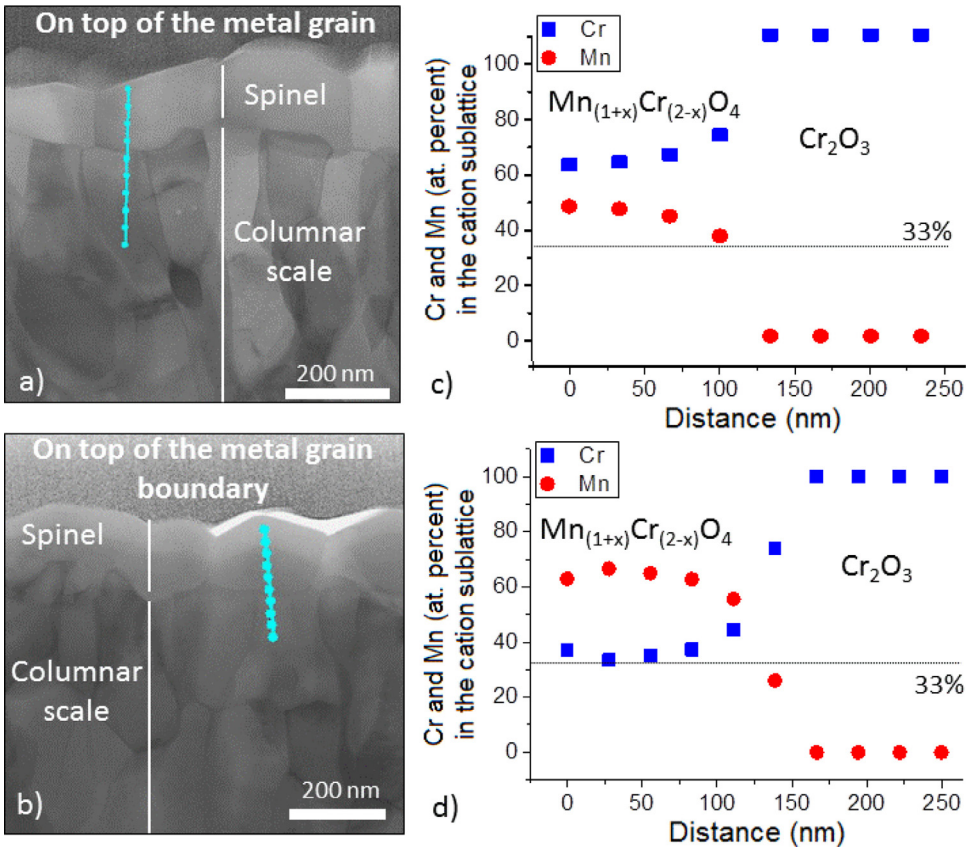

Fig. 3. Cross sections of the oxide scale formed on Ni–25Cr–1Mn oxidized 1 h in 200 Pa O_2(a) on top of a metal grain and (b) on top of a metal GB and respective composition profiles (EDS): (c) and (d).

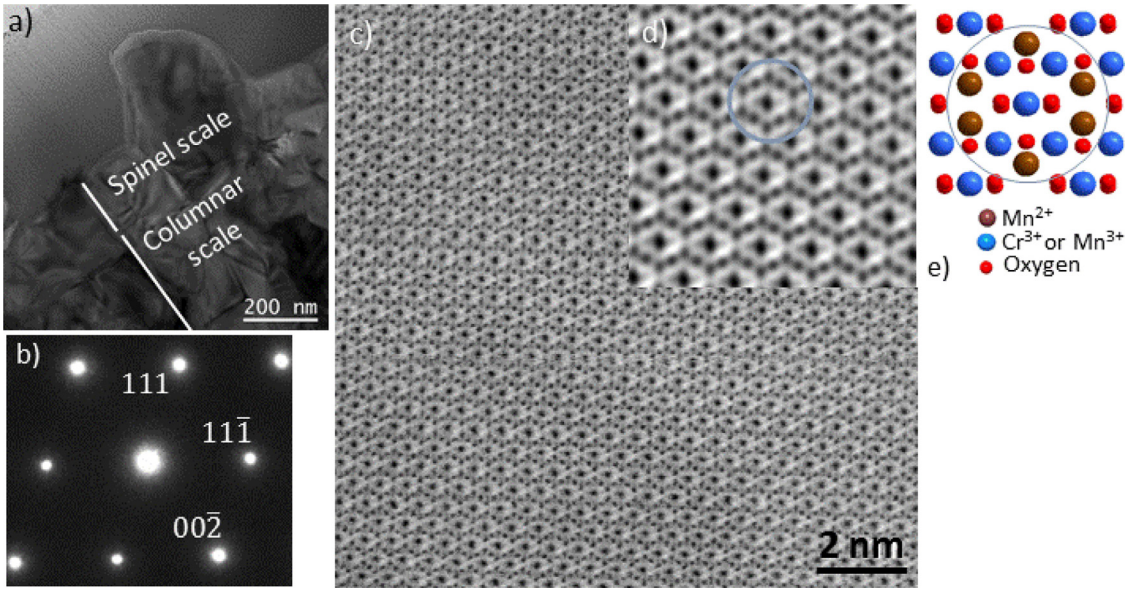

Fig. 4. (a) TEM bright field micrograph showing the selected area; (b) Selected area electron diffraction (SAED) pattern of the spinel crystallite; (c) and (d) High resolution STEM Filtered Annular Bright Field (ABF) micrographs and (e) Spinel structure (Fd-3m) along the [110] direction from Gautier et al. [25] showing the observed pattern (blue circled). (For interpretation of the references to color in this figure legend, the reader is referred to the web version of this article.)

atomic ratio. The spinel would be cubic from the composition $MnCr_2O_4$ to $Mn_{1.76}Cr_{1.24}O_4$ (%Mn/%Cr = 1.41), and tetragonal from $Mn_{1.76}Cr_{1.24}O_4$ up to Mn_3O_4 [22,23]. This transition was reported to be due to the Jahn-Teller effect of the Mn(III) on the spinel octahedral sites [22–25]. At a higher temperature, this transition is shifted towards a higher manganese concentration [21]. At the oxidation temperature used in the present study (1050 °C), a phase transformation should occur for $Mn_{2.7}Cr_{0.3}O_4$. The cubic structure determined in the present study confirms these previous results and demonstrates that a continuous solid solution exists between $MnCr_2O_4$ and at least $Mn_{2.04}Cr_{0.96}O_4$ at 1050 °C.

Finally, Annular Bright Field (ABF) and High Angle Annular Dark Field (HAADF) micrographs were collected on a well oriented spinel grain. This grain was oriented along the [110] direction. The ABF and HAADF micrographs were filtered to observe the atomic positions. On the presented ABF micrographs (Fig. 4c and c), each bright point should be associated with an atom column of light elements, i.e., to oxygen here, because the electrons' beam deviation is high for heavy elements. A repetitive pattern consisting of a very dark point in the centre of a hexagon formed of 10 dark points can be seen on the filtered ABF micrograph. These results can be directly compared to the atomic positions of $MnCr_2O_4$ as described by Gaultier et al. [25] (Fig. 4e). The pattern is circled in Fig. 4d and e for better illustration.

In summary, extensive HRTEM characterizations have been conducted to study the microstructure and the chemical composition of the oxide scale that develops on Ni–25Cr–xMn (x = 0.5, 1 and 1.5% wt) alloys in a 200 Pa O_2 environment at 1050 °C. It has been shown that the oxide scale is triplex. The oxide scale consists of two layers of chromia and one layer of a continuous spinel $Mn_{1+x}Cr_{2-x}O_4$, with x varying from 0 to 1.04. The spinel grains crystallize according to the cubic spinel structure (Fd-3m) under the conditions of the present work. On top of the metal grains, composition measurements made in the spinel near the chromia/spinel interface indicate a composition similar to $MnCr_2O_4$ regardless of the Mn concentration in the alloy. This finding demonstrates that equilibrium conditions are fulfilled at this interface. The equilibrium at the chromia/spinel interface can be written as follows ():

$$Mn_{(Cr_2O_3)} + Cr_2O_3 + {}^1/_2O_2 = MnCr_2O_4 \quad (1)$$

This can explain the changes in the semiconductive properties of Mn containing alloys [9]. In these conditions and according to Wagner Theory [26], the chromia growth is controlled by the oxygen activity gradient that establishes between the metal/oxide and chromia/spinel interfaces. The internal chromia layer exhibits an equiaxed grain structure, whereas the columnar chromia grains develop in the outer layer. Columnar microstructures were also recently observed in low oxygen environments [19,20], similar to the morphology obtained with Mn-containing alloys in the present work. This finding also supports the existence of the local equilibrium at the chromia/spinel interface.

Acknowledgments

We are pleased to acknowledge Dr. R. Podor, Dr. J. Lautru and Ms S. Migot for their assistance, respectively, with the oxidation experiments and the FIB lamella extraction. The authors thank the French National Research Agency (ANR) for the support of the PSEUDO project (Grant No. ANR-15-CE08-0021).

Declaration of Competing Interest

The authors declare that they have no known competing financial interests or personal relationships that could have appeared to influence the work reported in this paper.

References

[1] D.J. Young, High Temperature Oxidation and Corrosion of Metals, Elsevier, Oxford, 2008.
[2] D. Kim, C. Jang, W.S. Ryu, Oxid. Met. 71 (2009) 271–293.
[3] J. Zurek, D.J. Young, E. Essuman, M. Hänsel, H.J. Penkalla, L. Niewolak, W.J. Quadakkers, Mater. Sci. Eng. A 477 (2008) 259–270.
[4] T. Perez, L. Latu-Romain, R. Podor, J. Lautru, Y. Parsa, S. Mathieu, M. Vilasi, Y. Wouters, Oxid. Met. 89 (2018) 781–795.
[5] P. Kofstad, Nonstoichiometry, Diffusion and Electrical Conductivity in Binary Metal Oxides, Wiley, 1972.
[6] P. Kofstad, High Temperature Oxidation of Metals, John Wiley & Son, New York, 1966.
[7] D.L. Douglass, J.S. Armijo, Oxid. Met. 2 (1969) 207–231.
[8] T.D. Nguyen, J. Zhang, D.J. Young, Corros. Sci. 112 (2016) 110–127.
[9] X. Ledoux, S. Mathieu, M. Vilasi, Y. Wouters, P. Del-Gallo, M. Wagner, Oxid. Met. 80 (2013) 25–35.
[10] D.L. Douglass, J.S. Armijo, Oxid. Met. 2 (1969) 207–231.
[11] N. Hussain, K.A. Shahid, I.H. Khan, S. Rahman, Oxid. Met. 43 (1995) 363–378.
[12] N. Vaché, S. Cazottes, T. Douillard, C. Duret-Thual, F. Dupoiron, C. Augustin, P. Steyer, Oxid. Met. 91 (2019) 279–290.
[13] G.R. Holcomb, D.E. Alman, Scr. Mater. 54 (2006) 1821–1825.
[14] R. Podor, D. Pailhon, J. Ravaux, H.-P. Brau, Microsc. Microanal. 21 (2015) 307–312.
[15] L. Latu-Romain, Y. Parsa, S. Mathieu, M. Vilasi, M. Ollivier, A. Galerie, Y. Wouters, Oxid. Met. 86 (2016) 497–509.
[16] S. Lech, A. Kruk, A. Gil, G. Cempura, A. Agüero, A. Czyrska-Filemonowicz, Scr. Mater. 167 (2019) 16–20.
[17] L. Latu-Romain, Y. Parsa, S. Mathieu, M. Vilasi, A. Galerie, Y. Wouters, Corros. Sci. 126 (2017) 238–246.
[18] G. Zhou, Appl. Phys. Lett. 94 (2009) 201905.
[19] D. Simon, B. Gorr, H.J. Christ, Oxid. Met. 87 (2017) 417–429.
[20] M. Hänsel, V. Shemet, E. Turan, I. Kijatjin, D. Simon, B. Gorr, H.-J. Christ, ECS Trans. 66 (2015) 1–21.
[21] I.H. Jung, Solid State Ionics 177 (2006) 765–777.
[22] Z. Jirák, S. Vratislav, P. Novák, Phys. Status Solidi 50 (1978) K21–K24.
[23] Z. Jirák, S. Vratislav, J. Zajíček, Phys. Status Solidi 37 (1976) K47–K51.
[24] E. Povoden, A.N. Grundy, L.J. Gauckler, Z. Met. 97 (2006) 569–578.
[25] J.L. Gautier, J. Ortiz, G. Zelada, G. Poillerat, J. Chim. Phys. 86 (1989) 1889–1917.
[26] C. Wagner, Z. Phys. Chem. B B21 (1933) 25.